Journal of Photochemistry and Photobiology A: Chemistry 221 (2011) 77–83

Contents lists available at ScienceDirect

Journal of Photochemistry and Photobiology A: Chemistry

journal homepage: www.elsevier.com/locate/jphotochem

Transition metal ion substitution in titanosilicate ETS-10 for enhanced UV light photodegradation of methylene blue

Zhaoxia Ji [a], Mariam N. Ismail [a], Dennis M. Callahan Jr. [a], Juliusz Warzywoda [b], Albert Sacco Jr. [b,*]

[a] Department of Chemical Engineering, Northeastern University, Boston, MA 02115, USA
[b] Department of Chemical Engineering, Texas Tech University, Lubbock, TX 79409, USA

ARTICLE INFO

Article history:
Received 15 February 2011
Received in revised form 1 April 2011
Accepted 25 April 2011
Available online 30 April 2011

Keywords:
ETS-10
Methylene blue
Photocatalysis
Titanosilicate
Transition metals

ABSTRACT

Partial isomorphous substitution of transition metal (M = V, Cr, Mn, Fe, Co) ions in the titanosilicate ETS-10 framework (ETMS-10 with M/Ti ≈ 0.06 mol mol^{-1}) was carried out in efforts to enhance the photocatalytic activity of ETS-10 in the degradation of methylene blue (MB) under UV light (280–400 nm) irradiation. XRD, UV–vis, and EDX analyses suggested substitution of V^{4+}/V^{5+}, Cr^{3+}, Mn^{2+}, and Fe^{3+} for octahedral Ti^{4+}, and Co^{2+} for tetrahedral Si^{4+} in the ETS-10 framework. All ETMS-10 samples showed lower bandgap energies (E_g = 3.79–3.90 eV) than unmodified ETS-10 (E_g = 3.96 eV), and exhibited absorption features in the visible light region. These samples showed higher photocatalytic activities in photodegradation of MB (pseudo-first-order reaction rate constants, k = 0.016–0.055 min^{-1}) than unmodified ETS-10 (k = 0.008 min^{-1}), and the activities decreased in the order: ETCoS-10 > ETCrS-10 ≈ ETFeS-10 > ETMnS-10 ≈ ETVS-10 > unmodified ETS-10. This was hypothesized to be due in part to the lower bandgap energies of ETMS-10 samples compared to that of unmodified ETS-10, as well as the introduction of midgap states with transition metal ions replacing Ti^{4+}, and different d electron configurations of transition metal ions substituted in the ETS-10 framework.

1. Introduction

Titanosilicate ETS-10 is a crystalline microporous (pore size 4.9 Å × 7.6 Å) material with a framework composed of corner-sharing TiO_6 octahedra and SiO_4 tetrahedra [1]. The framework of ETS-10 contains monatomic linear semiconducting ···Ti–O–Ti–O–Ti··· chains that are effectively separated from one another by the surrounding silica matrix [2], and are hypothesized to be a quantum-confined form of titania (TiO_2) with a bandgap energy of 4.03 eV [3]. This has made ETS-10 a possible UV light photocatalyst in photodegradation of various organic chemicals [4–9].

The photocatalytic activity of ETS-10 is limited to a large extent by its high bandgap energy. Recently, various attempts have been made to improve the photocatalytic performance of this material in the UV light region, and extend its activity to the visible light region. These include post-synthesis acid treatment [5], ion exchange with NH_4^+ [10] and various transition metal ions [7], encapsulation of CdS nanoparticles in the ETS-10 micropore system [11], partial isomorphous substitution of Ti or Si with some transition metal ions [7,8], and partial substitution of O with anionic species of S, C, and N [12].

Although several transition metal ions (i.e., V [8,13], Nb [14], Fe [15,16], Cr [7,17], Co [7,18], and Zr [19]) have been partially isomorphously substituted in the ETS-10 framework, only ETS-10 samples substituted with chromium, cobalt, and vanadium [7,8] have been investigated in photocatalysis. These substitutions were carried out following the general method that was first disclosed in a patent [20], which claimed substitutions of these and other metal ions for octahedral and/or tetrahedral sites in ETS-10 using the appropriate metal salts in ETS-10 synthesis mixtures. Vanadium-substituted ETS-10 (ETVS-10) samples had higher activity than unmodified ETS-10 in the photocatalytic polymerization of ethylene in the combined UV and visible light regions [8]. This was attributed to lowering of the bandgap energy and appearance of photocatalytically active absorbance at 450 nm due to charge-transfer transition associated with octahedrally coordinated V^{5+} in the framework of ETVS-10 [8]. Calcined at 773 K chromium (ETCrS-10) and cobalt (ETCoS-10) substituted ETS-10 samples showed the same activity as unmodified ETS-10 for the photocatalytic decomposition of acetaldehyde in the UV light region [7]. Based on these limited data, the effects of transition metal ion substitution in the ETS-10 framework on the photocatalytic activity of resulting ETS-10 materials, and thus the role that the substituted transition metal ions play in affecting the photocatalytic performance of ETS-10 under UV light irradiation is unclear.

Incorporation of transition metal ions in the crystal lattice has been used in efforts to improve the photocatalytic activity of TiO_2

* Corresponding author. Tel.: +1 806 742 3451; fax: +1 806 742 3493.
E-mail addresses: al.sacco-jr@ttu.edu, asacco@coe.neu.edu (A. Sacco Jr.).

1010-6030/$ – see front matter © 2011 Elsevier B.V. All rights reserved.
doi:10.1016/j.jphotochem.2011.04.027

[21–24]. UV–vis spectroscopic characterization of thus modified TiO_2 samples often shows additional absorption in the visible light region, and the red shift of the intrinsic absorption edge of TiO_2. These changes in spectral features stem from the introduction of the transition metal ion energy levels within the bandgap of TiO_2 [21,23]. The red shift in the bandgap energy is likely due to the introduced new charge-transfer transitions between the transition metal ion d electrons and the conduction or the valence band of TiO_2. The absorption band(s) that appear in the visible light region may be due to d–d transitions in the introduced transition metal ions, and may also be due to charge transfer between the introduced transition metal ions and the conduction (or valence) band of TiO_2 [21–23]. However, despite the enhanced light absorption in the UV and visible light regions observed for the modified TiO_2 samples, their photocatalytic activities under UV or visible light irradiation are not always increased. This was proposed [21,24] to be because the incorporated transition metal ions should act as both electron traps and hole traps to be photoactive. Trapping either an electron or a hole alone may not be as effective, because the immobilized charge carrier quickly recombines with its mobile counterpart. In ETS-10 this recombination may be further hindered, owing to hypothesized quantum wires providing a pathway for electrons to rapidly move away from the vicinity of the hole.

In this investigation, degradation of a model compound, methylene blue (MB), was systematically investigated under UV light irradiation on the unmodified and isomorphously substituted with V^{4+}/V^{5+}, Cr^{3+}, Mn^{2+}, Fe^{3+}, or Co^{2+} ETS-10 samples, and the photocatalytic results compared with the optical properties of these materials. The incorporation of transition metal ions in the ETS-10 framework together with the ETS-10 structure (i.e., quantum wires) can improve the photocatalytic performance of ETS-10 under UV light irradiation, and the possible role of individual metal ions in the UV light photocatalysis on ETS-10 is further elucidated.

2. Experimental methods

2.1. ET(M)S-10 synthesis and characterization

The unmodified ETS-10 crystals [25] and transition metal ion-substituted ETS-10 [7] (ETMS-10, M = V, Cr, Mn, Fe, Co) crystals were hydrothermally synthesized according to the literature procedures. The synthesis mixture composition was $5.2Na_2O{:}0.5\,K_2O{:}1.0TiO_2{:}5.5SiO_2{:}113H_2O$. To synthesize ETMS-10 crystals, the transition metal salts such as $VOSO_4{\cdot}5H_2O$ (97%, Aldrich), $Cr(NO_3)_3{\cdot}9H_2O$ (99%, Aldrich), $Mn(NO_3)_2{\cdot}5H_2O$ (98%, Aldrich), $Fe(NO_3)_3{\cdot}9H_2O$ (98+%, Aldrich), or $Co(NO_3)_2{\cdot}6H_2O$ (98+%, Aldrich) were added to the solution containing N-Brand sodium silicate (28.59% SiO_2, 8.88% Na_2O, PQ), sodium chloride (NaCl, 99.0%, Sigma), potassium chloride (KCl, 99.0%, Fisher), and deionized water (resistivity >18 MΩ cm). To this solution anatase powder (99% TiO_2, Aldrich) was added, and the resulting mixture was vigorously hand-shaken for 5 min before transferring it into Teflon-lined stainless steel autoclaves. For all transition metal (M) ions used, the mixture molar M/Ti ratio was 0.05. Synthesis of unmodified ETS-10 was accomplished using the same procedure but without transition metal salts. After crystallization at 503 K for 3–6 days, the products were cooled to room temperature, filtered and washed with 1 L of deionized water, and air-dried overnight at 353 K.

X-ray powder diffraction (XRD, Bruker D5005 diffractometer equipped with a curved graphite crystal diffracted beam monochromator and a NaI scintillation detector, Cu Kα radiation, 40 kV, 30 mA) was used to determine purity of ET(M)S-10 products. Field emission scanning electron microscopy (FE-SEM, Hitachi S-4700 FE-SEM, accelerating voltage 2 kV, beam current 10 μA) was used to image crystal morphology. Energy dispersive X-ray spectroscopy (EDX, Phoenix EDAX X-ray analyzer equipped with Sapphire super ultra thin window detector attached to the Hitachi S-4700 FE-SEM, accelerating voltage 20 kV, beam current 10 μA) was conducted to estimate the amount of transition metal ions present in ETMS-10 crystals. Diffuse reflectance UV–vis spectroscopy (Cary 5000 UV–vis–NIR spectrometer equipped with a Praying Mantis accessory, powdered Spectralon™ reference material) was used to obtain optical properties and determine band gap energies of the investigated samples. An API Aerosizer LD equipped with an API Aero-Disperser dry powder dispersion system (TSI, Inc., Particle Instruments/Amherst) was used to measure the particle size distributions (PSDs) of the investigated samples. For these measurements, the average density of the samples was assumed to be 1750 kg m^{-3} [26]. Based on the PSD data, the API Aerosizer software was used to calculate the external specific surface area (S_{EXT}) of each sample. This quantity is defined by the software as the total surface area of the number of particles whose total volume equals 1 cm^3, and the results for S_{EXT} are given in $m^2\,g^{-1}$.

2.2. Photocatalytic degradation of MB

All photocatalytic experiments were conducted at room temperature (298 K ± 3 K) in a 200 mL stirred Pyrex beaker using a crystal suspension of 500 mg L^{-1} in a 100 mL aqueous methylene blue (MB, Sigma–Aldrich) solution, which had a concentration of 10 mg L^{-1} and a pH of 5.4. This pH was determined from preliminary experiments in which pH were adjusted by adding 0.1 M aqueous NaOH solution or 0.1 M aqueous acid solutions to an ETS-10 suspension. These preliminary trials showed the highest activity occurred at pH values in the range 4.0–5.4. Further preliminary experimentation showed that the rate of MB conversion did not change above 750 rpm for the most active samples tested. Thus, a rate of 1000 rpm was utilized to eliminate external mass transfer as well as to uniformly disperse ET(M)S-10 crystals, and to aerate the mixture during the light irradiation to avoid photobleaching of MB that occurs at insufficient dissolved oxygen concentrations [27,28]. Magnetic stirring of suspensions in the dark for 1 h prior to irradiation achieved adsorption/desorption equilibrium. Utilizing these experimental conditions without light irradiation, no degradation of MB was observed. To achieve solution irradiation, a 500 W Xe arc lamp (Oriel Model 66924) was positioned 10 cm from the top surface of reaction mixture, and the light was passed through a dichroic mirror (280–400 nm) to ensure UV light exposure. The degradation of MB during photocatalysis was monitored using a Cary 5000 UV–vis–NIR spectrometer (sample size 4 mL). The concentration of MB in each sample was determined from the intensity of the absorbance maximum at ~664 nm due to MB in the UV–vis spectrum [27].

3. Results and discussion

3.1. Characterization of ET(M)S-10

XRD analysis showed highly crystalline ETS-10 as the only phase in the unmodified sample as well as in all transition metal ion-substituted (i.e., ETMS-10) samples; no impurity phases containing any of the transition metals were detected. All ETMS-10 samples showed a slight shift of XRD peaks compared to unmodified ETS-10 (expansion of the XRD patterns around the most intense peak at ~24.7° 2θ is illustrated in Fig. 1). The peaks for ETCrS-10, ETMnS-10, ETFeS-10, and ETCoS-10 shifted to lower angle (Fig. 1). Such a shift for ETCrS-10 and ETFeS-10 can be expected considering the replacement of the smaller octahedral Ti^{4+} (ionic radius 0.745 Å [29]) in the ETS-10 framework by either the larger octahedral Cr^{3+} (ionic radius 0.755 Å [29]) or the larger octahedral Fe^{3+} (ionic radius

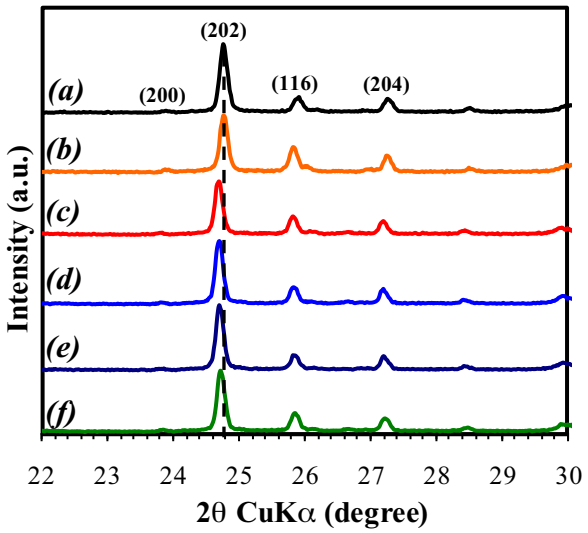

Fig. 1. XRD patterns of: (a) unmodified ETS-10, (b) ETVS-10, (c) ETCrS-10, (d) ETMnS-10, (e) ETFeS-10, and (f) ETCoS-10.

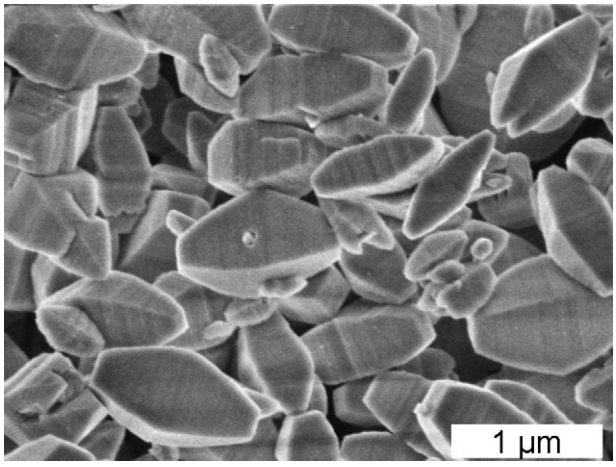

Fig. 2. FE-SEM image of the unmodified ETS-10 crystals.

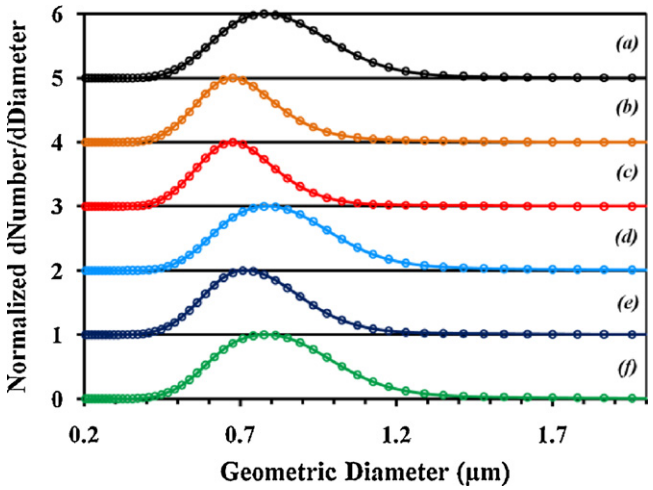

Fig. 3. PSDs of: (a) ETCrS-10, (b) ETVS-10, (c) ETFeS-10, (d) unmodified ETS-10, (e) ETCoS-10, and (f) ETMnS-10.

0.785 Å [29]), giving slightly larger unit cells of these substituted ETS-10 samples compared to that for unmodified ETS-10. Such replacement in ETS-10 was reported before [15–17]. By analogy, a similar lower angle peak shift for ETMnS-10 can be interpreted as a result of increase of its unit cell volume due to replacement of Ti^{4+} in the ETS-10 framework by the larger octahedral Mn^{2+} (ionic radius 0.97 Å [29]). In agreement with previous results [18], the lower angle peak shift for ETCoS-10 was taken to indicate the substitution of larger tetrahedral Co^{2+} (ionic radius 0.72 Å [29]) for the much smaller tetrahedral Si^{4+} (ionic radius 0.4 Å [29]) in the ETS-10 framework. The opposite, very slight shift of XRD peaks to higher angle for ETVS-10 (Fig. 1), i.e., smaller unit cell volume, is likely due to the smaller ionic radii of octahedral V^{4+} (0.72 Å) and octahedral V^{5+} (0.68 Å) [29] that replace larger Ti^{4+} in the ETS-10 framework [8].

FE-SEM analysis showed that crystals in all ETMS-10 samples (not shown for brevity) had the same elongated truncated bipyramidal morphology as the unmodified ETS-10 crystals (Fig. 2). However, the colors of these ETMS-10 crystals were different from the white color of unmodified ETS-10, and depended on the type of substituted transition metal ion: ETVS-10 was grayish, ETCrS-10 was bright green, ETMnS-10 and ETCoS-10 were pink, whereas ETFeS-10 appeared light orange. FE-SEM analysis revealed also that individual crystals in all ETMS-10 samples did not exceed the dimensions of the unmodified ETS-10 crystals (i.e., maximum length no larger than ~1.5 μm, maximum width no larger than ~1.0 μm). PSD analysis confirmed these visual observations (Fig. 3). PSDs of ETMnS-10 and ETCoS-10 samples were practically identical to that of the unmodified ETS-10 sample. Crystals in the ETCrS-10, ETVS-10, and ETFeS-10 sample populations were slightly smaller on average than the unmodified ETS-10 crystals (Fig. 3). The external specific surface areas (S_{EXT}) of all ET(M)S-10 samples investigated were calculated based on the PSD data using the Aerosizer software, and the S_{EXT} values are shown in Table 1. The S_{EXT} values reflect the PSD trends shown in Fig. 3.

Also, Table 1 shows the results of EDX analysis performed to determine the transition metal content (M/Ti, M = V, Cr, Mn, Fe, Co) and Si/Ti ratios in ETMS-10 crystals. All transition metal ions investigated appeared to replace Ti to approximately the same extent in ETMS-10 samples (M/Ti ≈ 0.06). Also, the crystal Si/Ti ratios measured for all ETMS-10 samples (Table 1) were identical within experimental error to that obtained for unmodified ETS-10. In principle, the substitution of Si by Co in ETCoS-10 [18] should result in a lower crystal Si/Ti ratio in this material compared to unmodified ETS-10, whereas the substitution of Ti by V, Cr, and Fe in ETVS-10 [8], ETCrS-10 [17], and ETFeS-10 [15], respectively, should result in higher crystal Si/Ti ratios in these materials compared to unmodified ETS-10. However, the relatively large error associated with EDX analysis for the Si/Ti ratios (±0.2 mol mol^{-1}, Table 1), and the low transition metal content in all ETMS-10 samples (M/Ti ≈ 0.06 mol mol^{-1}, Table 1) did not allow the unambiguous assignment of transition metal ion location in these samples based on these EDX results.

A systematic UV–vis spectroscopic analysis was performed on ETMS-10 samples to determine the oxidation states of transition metal ions. The asymmetric absorption band in the UV light region in the spectra collected for unmodified ETS-10 as well as all ETMS-10 samples (Fig. 4a) has been shown to have three components [30,31]. These components are due to the O^{2-} to Ti^{4+} charge-transfer (CT) transitions: the localized CT transitions in the Ti–O–Si groups, the delocalized CT transitions along the ···Ti–O–Ti–O–Ti··· chains, and the localized CT transitions caused by defects in the chains [31]. Unlike unmodified ETS-10, all ETMS-10 samples exhibited noticeable absorption in the visible light region, in addition to displaying a small red shift of the absorption edge from that of the unmodified ETS-10 sample (Fig. 4a). These features are clearly shown in the absorbance spectra re-plotted in the narrower

Table 1
The external specific surface areas (S_{EXT}), crystal M/Ti and Si/Ti ratios, bandgap energies (E_g), and pseudo-first-order reaction rate constants for the photodegradation of MB (k) for different ET(M)S-10 (M = V, Cr, Mn, Fe, Co) samples.

Sample	S_{EXT} ($m^2\ g^{-1}$)[a]	M/Ti (mol mol^{-1})[b]	Si/Ti (mol mol^{-1})[b]	E_g (eV)[c]	k (min^{-1})[d]
ETS-10	3.6 ± 0.1	0	5.5 ± 0.2	3.96 ± 0.02	0.008 ± 0.001
ETVS-10	4.2 ± 0.1	0.063 ± 0.004	5.7 ± 0.2	3.90 ± 0.02	0.016 ± 0.002
ETCrS-10	4.3 ± 0.1	0.060 ± 0.004	5.2 ± 0.2	3.86 ± 0.02	0.042 ± 0.004
ETMnS-10	3.5 ± 0.1	0.060 ± 0.004	5.2 ± 0.2	3.82 ± 0.02	0.020 ± 0.002
ETFeS-10	3.9 ± 0.1	0.063 ± 0.002	5.7 ± 0.2	3.79 ± 0.02	0.034 ± 0.003
ETCoS-10	3.5 ± 0.1	0.055 ± 0.003	5.4 ± 0.2	3.82 ± 0.02	0.055 ± 0.005

[a] Calculated from the PSD data.
[b] Calculated from the EDX data.
[c] Calculated from the UV–vis data.
[d] Calculated from the MB photodegradation kinetics data.

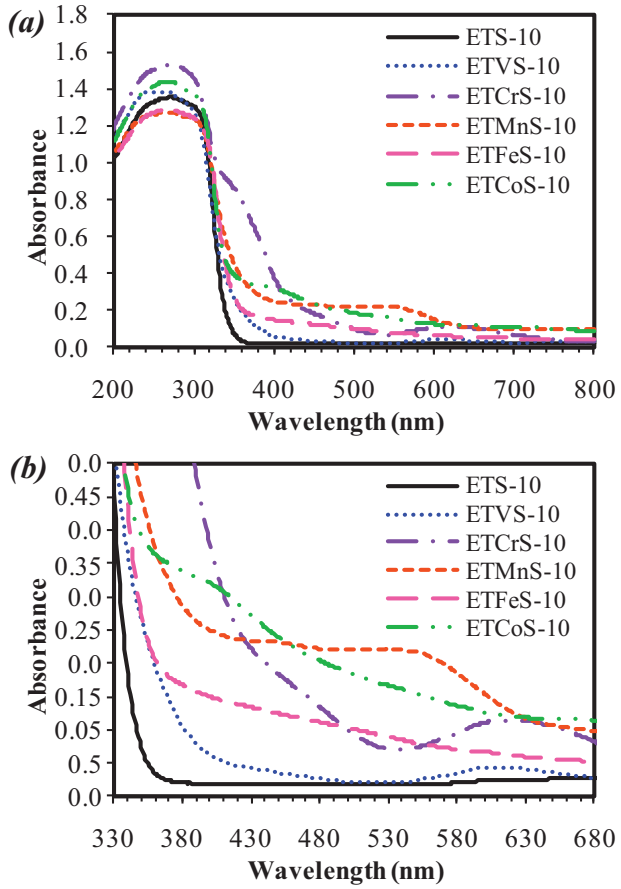

Fig. 4. UV–vis absorption spectra of the unmodified ETS-10 and different ETMS-10 (M = V, Cr, Mn, Fe, Co) samples in the: (a) 200–800 nm and (b) 330–700 nm range.

wavelength range (Fig. 4b). The ETVS-10 sample exhibited (Fig. 4b) a broad absorption band centered at ~450 nm due to charge-transfer transition associated with distorted octahedral V^{5+}, and absorption band centered at ~600 nm corresponding to d–d transition in distorted octahedral V^{4+} in the ETS-10 framework [8]. This suggested two oxidation states (V^{4+} and V^{5+}) for vanadium substituted for Ti^{4+} in the ETS-10 framework. The two absorption bands centered at ~450 nm and ~625 nm for ETCrS-10 (Fig. 4b) are characteristic of d–d transitions in octahedral Cr^{3+} in the ETS-10 framework [17], thus suggesting the substitution of Cr^{3+} for Ti^{4+} in ETCrS-10. The ETMnS-10 sample showed strong absorption band(s) at 400–650 nm (Fig. 4). The bands centered at ~420 nm, ~500 nm, and ~610 nm are characteristic for d–d transitions of the octahedrally coordinated Mn^{2+} [32,33]. This suggested incorporation of Mn^{2+} in the framework of ETMnS-10. Significant absorption in the visible light region up to ~650 nm was observed in ETFeS-10 sample, although no distinct absorption band(s) could be distinguished in this energy range (Fig. 4a). In addition, a noticeable red shift of the absorption edge from that for the unmodified ETS-10 sample, together with a considerable tailing of the absorption due to charge-transfer transition into the visible light region was observed for ETFeS-10 (Fig. 4b). Similar results were obtained for the Fe^{3+}-substituted ETS-10 by Eldewik et al. [15], who attributed these results to octahedrally coordinated Fe^{3+} that replaces Ti^{4+} in the ETS-10 framework. In ETCoS-10, the broad absorption bands observed at ~390 nm and 500–700 nm (Fig. 4b) have been assigned to tetrahedrally coordinated Co^{2+} that replaces Si^{4+} in the ETS-10 framework [18]. Thus, the UV–vis spectroscopic results, together with XRD and EDX analyses, strongly suggested the successful incorporation of all transition metal ions investigated here in the ETS-10 framework. The bandgap energies (E_g) were determined from the UV–vis spectra using the method described in literature [8,34], and the E_g values are shown in Table 1. As illustrated in Table 1, all ETMS-10 samples showed somewhat lower bandgap energies (3.79–3.90 eV) compared to that (3.96 eV) of the unmodified ETS-10 sample.

3.2. Photocatalytic degradation of MB

For all ET(M)S-10 samples the intensity of MB absorbance maximum at ~664 nm decreased with increasing reaction time and blue-shifted when measured at longer reaction times (an example of the temporal changes for the ~664 nm peak during MB photodegradation on ETFeS-10 during the first 11 min is shown in Fig. 5). This suggested oxidative N-demethylation of the dimethylamino groups in MB occurring together with oxidative degradation of the MB chromophore [27]. Formation of N-demethylated intermediates implied [27] that the ETS-10-sensitized photoreduction of MB possible during the UV light activation of a photocatalyst [28] did not occur in our investigation. Thus, the concentration of dissolved molecular oxygen in the reaction mixtures, and the rate of trapping the photogenerated conduction band electrons by oxygen adsorbed on the ETS-10 surface appeared to be sufficient [28] to result in the photodegradation of MB.

The photodegradation reaction appeared to be first-order with respect to MB, as indicated by the photodegradation kinetics data (Fig. 6). This is in agreement with observations of others [27,35]. The pseudo-first-order reaction rate constants (k) were determined based on the data in Fig. 6, and the k values are shown in Table 1. All these k values were larger than the direct UV light photolysis rate constant determined for MB (~0.005 min^{-1}) under the same reaction conditions. Therefore, all ET(M)S-10 samples were active in the photodegradation of MB under UV light irradiation, and their activities increased in the order: unmodified ETS-10 < ETVS-10 ≈ ETMnS-10 < ETFeS-10 ≈ ETCrS-10 < ETCoS-10. These activities (k values) did not correlate with the S_{EXT} values of different

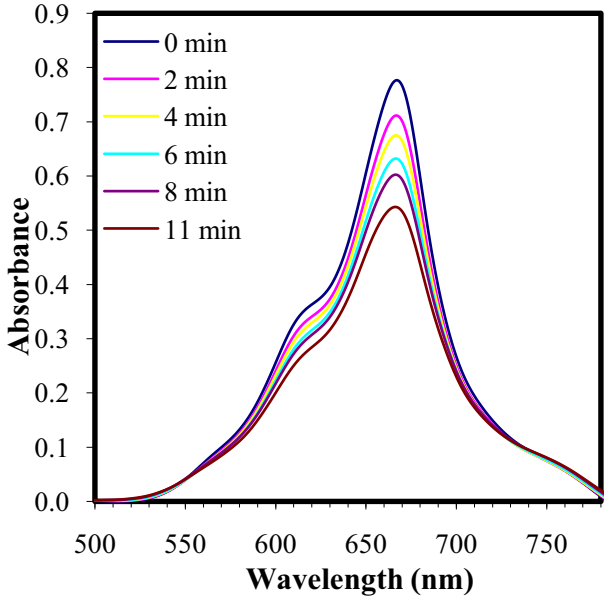

Fig. 5. Temporal spectral changes of MB in aqueous ETFeS-10 suspension under 280–400 nm UV light irradiation. Absorption maximum at ~664 nm is due to the methylene blue monomer, absorption shoulder at ~615 nm is due to the methylene blue dimer [28].

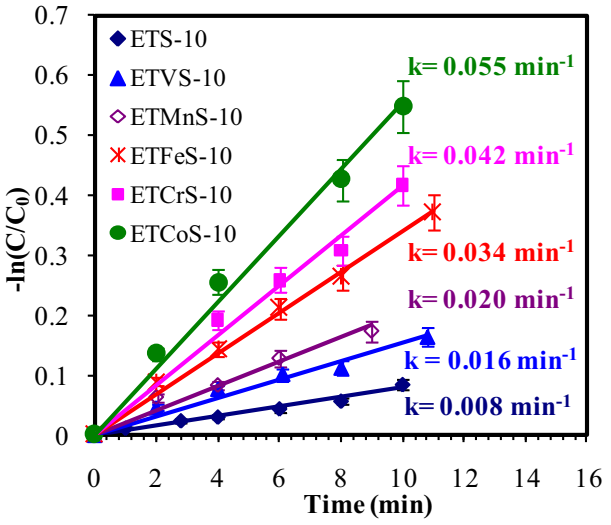

Fig. 6. The photocatalytic degradation kinetics of MB on the unmodified ETS-10 and different ETMS-10 (M = V, Cr, Mn, Fe, Co) samples under 280–400 nm UV light irradiation.

ET(M)S-10 samples (Table 1), indicating other factors were evidently more important in affecting the activity of these samples.

In the UV light range investigated here, the photodegradation of MB occurs mainly via a photocatalytic pathway [28,36], where the suprabandgap photon-generated conduction band electrons and valence band holes from the ET(M)S-10 semiconductor samples participate directly or indirectly via formation of reactive oxygen radicals (e.g., $HO^{\bullet}$, $HO_2^{\bullet}$) in the degradation of MB [27]. Thus, the higher photocatalytic activities of ETMS-10 samples compared to that of unmodified ETS-10 may in part be attributed to a somewhat broader UV irradiation range utilization by the substituted ETS-10 samples, as indicated by the lower bandgap energies of all ETMS-10 samples compared to that of unmodified ETS-10. However, the order of decreasing activity (decreasing k values) of individual ETMS-10 samples did not correlate with the order of increasing

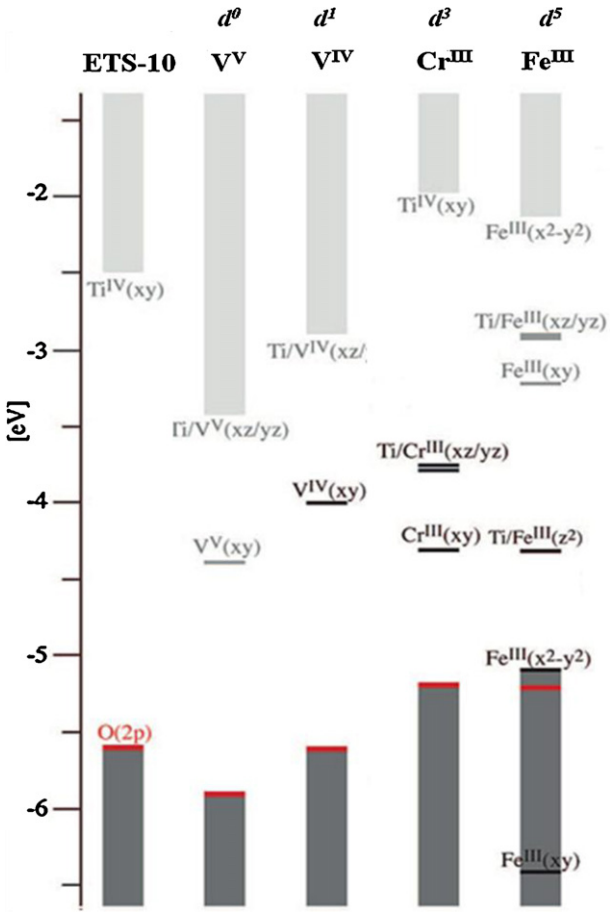

Fig. 7. Electronic structures of ETS-10 and 33% substituted [M/Ti] models for d^{0-5} metals (M = V, Cr, Fe) estimated using DFT orbital energies. Red lines indicate the position of the O(2p) energy levels. Black and gray lines represent the occupied and unoccupied midgap states, respectively. Light and dark gray rectangles represent the unoccupied conduction band and occupied valence band states, respectively. (For interpretation of the references to color in this figure legend, the reader is referred to the web version of this article.)
Adapted from Shough et al. [38].

E_g values for these samples (Table 1). In fact, the results shown in Fig. 6 showed that the photocatalytic activity of ETMS-10 samples varied greatly with the type of transition metal ion substituted in the ETS-10 framework. Thus, the differences in photoreactivity of different ETMS-10 samples are related to the differences in the electronic structure of ETS-10 substituted with different transition metal ions, and different d electronic configurations of these ions. This is because just as recombination of photogenerated electrons and holes is detrimental to the performance of a semiconductor photocatalyst [37], the increase of activity of such a photocatalyst may be achieved by reducing the rate of electron-hole recombination via incorporation of the appropriate (i.e., "photoactive") transition metal ions in the crystal lattice [21,24], recognizing that the effect, if any, of quantum wires should be constant regardless of metal substitution.

Transition metal ion substitutions for the octahedral Ti^{4+} in the ETS-10 framework investigated here which were also modeled (i.e., V^{5+}, V^{4+}, Cr^{3+}, and Fe^{3+}) were shown to result in midgap states (i.e., states that are positioned above the valence band or below the conduction band) [38]. The electronic structures modeled in [38] relevant to the present investigation are shown in Fig. 7. These midgap states can behave as electron or hole trapping sites along the ···Ti–O–Ti–O–Ti··· chains in ETS-10, depending on whether these states are unoccupied or occupied, respectively. Ions such as

Fe^{3+} and Cr^{3+} can act as both electron and hole traps [38]; whereas V^{4+} and Mn^{2+} can only act as hole traps, and V^{5+} [38] can only behave as electron traps. Ions with closed-shell electronic configurations (such as V^{5+}, electronic configuration: $1s^2 2s^2 2p^6 3s^2 3p^6$, i.e., [Ar]) have little effect on the observed photocatalytic activity [21]. UV–vis spectroscopic analysis suggested the presence of V^{4+} and V^{5+} in the framework of ETVS-10 (Fig. 4); however, previous investigations [8] have shown more V^{5+} to be present throughout the framework than V^{4+}. Therefore, the relatively low activity of ETVS-10 can be attributed to the closed-shell electronic configuration of V^{5+}. As reported by Choi et al. [21] and Zhang et al. [24] trapping either only electrons or only holes is not effective because the immobilized charge species can easily recombine with their mobile counterparts. Therefore, the relatively low activity of ETMnS-10 can be due to the fact that Mn^{2+} cannot serve as electron trap. In contrast, Fe^{3+} in ETFeS-10 and Cr^{3+} in ETCrS-10 can serve as both electron and hole traps, and therefore would be expected to lead to higher photocatalytic activity, as observed (Fig. 6). Although Fe^{3+} and Cr^{3+} have similar energy levels (Fig. 7) as well as the same oxidation state, Cr^{3+} appeared to be somewhat more effective than Fe^{3+} for ETS-10 modifications for use in MB photodegradation. Since photogenerated holes prefer states of higher energy, a hole trapped in the localized Cr^{III} (d_{xy}) can easily transition into the more delocalized d_{xz}/d_{yz} state (Fig. 7), which can be more effective in transporting the photogenerated holes to the active sites of ETS-10 [38]. This would likely make ETCrS-10 more active than ETFeS-10, as observed (Fig. 6). The reasons for the highest photocatalytic activity of ETCoS-10 among all ETMS-10 samples investigated here are at present unclear but the photodegradation performance of this sample is evidently related to the presence/tetrahedral coordination of Co^{2+} in the ETS-10 framework.

4. Conclusions

Titanosilicate ETS-10 has been modified by V^{4+}/V^{5+}, Cr^{3+}, Mn^{2+}, and Fe^{3+}, which partially substituted for octahedral Ti^{4+}, and by Co^{2+} which partially replaced tetrahedral Si^{4+} in the framework. All these transition metal (M) ions substituted to approximately the same extent in ETMS-10 samples (M/Ti ≈ 0.06). Isomorphous substitutions decreased ETS-10 bandgap energy from 3.96 eV for unmodified ETS-10 to 3.79–3.90 eV for ETMS-10 samples, and resulted in the appearance of absorption in the visible light region. All ETMS-10 samples (k = 0.016–0.055 min^{-1}) were more active than unmodified ETS-10 (k = 0.008 min^{-1}) in the degradation of MB under 280–400 nm UV light irradiation. Significant differences in the photoreactivity of ETS-10 substituted with different transition metal ions were partially attributed to the effect of different bandgap energies of the substituted samples. Also, in the case of isomorphous substitution for Ti^{4+} in the framework, these differences were hypothesized to be related to the effect of different energy levels of the introduced transition metal ions within the ETS-10 framework as well as their different d electronic configurations.

Acknowledgement

The authors thank NASA for financial support.

References

[1] S.M. Kuznicki, Large-pored crystalline titanium molecular sieve zeolites, US Patent 4,853,202 (1989).
[2] M.W. Anderson, O. Terasaki, T. Ohsuna, A. Philippou, S.P. MacKay, A. Ferreira, J. Rocha, S. Lidin, Structure of the microporous titanosilicate ETS-10, Nature 367 (1994) 347–351.
[3] E. Borello, C. Lamberti, S. Bordiga, A. Zecchina, C.O. Areán, Quantum-size effects in the titanosilicate molecular sieve, Appl. Phys. Lett. 71 (1997) 2319–2321.
[4] P. Calza, C. Pazé, E. Pelizzetti, A. Zecchina, Shape-selective photocatalytic transformation of phenols in an aqueous medium, Chem. Commun. (2001) 2130–2131.
[5] F.X. Llabrés i Xamena, P. Calza, C. Lamberti, C. Prestipino, A. Damin, S. Bordiga, E. Pelizzetti, A. Zecchina, Enhancement of the ETS-10 titanosilicate activity in the shape-selective photocatalytic degradation of large aromatic molecules by controlled defect production, J. Am. Chem. Soc. 125 (2003) 2264–2271.
[6] Y.K. Krisnandi, P.D. Southon, A.A. Adesina, R.F. Howe, ETS-10 as a photocatalyst, Int. J. Photoenergy 5 (2003) 131–140.
[7] S. Uma, S. Rodrigues, I.N. Martyanov, K. Klabunde, Exploration of photocatalytic activities of titanosilicate ETS-10 and transition metal incorporated ETS-10, Micropor. Mesopor. Mater. 67 (2004) 181–187.
[8] M.J. Nash, S. Rykov, R.F. Lobo, D.J. Doren, I. Wachs, Photocatalytic activity of vanadium-substituted ETS-10, J. Phys. Chem. C 111 (2007) 7029–7037.
[9] Y. Shiraishi, D. Tsukamoto, T. Hirai, Selective photocatalytic transformations on microporous titanosilicate ETS-10 driven by size and polarity of molecules, Langmuir 24 (2008) 12658–12663.
[10] Y.K. Krisnandi, R.F. Howe, Effects of ion-exchange on the photoreactivity of ETS-10, Appl. Catal. A 307 (2006) 62–69.
[11] G. Guan, T. Kida, K. Kusakabe, K. Kimura, E. Abe, A. Yoshida, Photocatalytic activity of CdS nanoparticles incorporated in titanium silicate molecular sieves of ETS-4 and ETS-10, Appl. Catal. A 295 (2005) 71–78.
[12] M.V. Shankar, J. Ye, Inorganic alkaline-sols as precursors for rapid synthesis of ETS-10 microporous titanosilicates and their photocatalytic reforming of methanol under visible-light irradiation, Catal. Commun. 11 (2009) 261–265.
[13] P. Brandão, A.A. Valente, J. Rocha, M.W. Anderson, Synthesis, characterization and catalytic activity of vanadium-containing ETS-10, Stud. Surf. Sci. Catal. 142 (2002) 327–334.
[14] J. Rocha, P. Brandão, J.D. Pedrosa de Jesus, A. Philippou, M.W. Anderson, Synthesis and characterization of microporous titanoniobosilicate ETNbS-10, Chem. Commun. (1999) 471–472.
[15] A. Eldewik, V. Luca, N.K. Singh, R.F. Howe, Iron substitution in the microporous titanosilicate ETS-10, in: Proceedings of the 12th International Zeolite Conference, vol. 3, Materials Research Society, 1999, pp. 1507–1514.
[16] K. Lázár, A.J. Chandwadkar, P. Fejes, J. Čejka, A.V. Ramaswamy, Valency changes of iron and tin in framework-substituted molecular sieves investigated by in situ Mossbauer spectroscopy, J. Radioanal. Nucl. Chem. 246 (2000) 143–148.
[17] P. Brandão, A. Philippou, A. Valente, J. Rocha, M. Anderson, Synthesis and characterisation of chromium-substituted ETS-10, Phys. Chem. Chem. Phys. 3 (2001) 1773–1777.
[18] A. Eldewik, R.F. Howe, Cobalt substitution in ETS-10, Micropor. Mesopor. Mater. 48 (2001) 65–71.
[19] D. Vuono, C.C. Pavel, P. De Luca, J.B. Nagy, A. Nastro, Influence of zirconium on the crystallization of ETS-10 molecular sieve, J. Therm. Anal. Calorim. 80 (2005) 585–590.
[20] S.M. Kuznicki, K.A. Trush, Large-pored molecular sieves containing at least one octahedral site comprising titanium and at least silicon as a tetrahedral site, US Patent 5,208,006 (1993).
[21] W. Choi, A. Termin, M.R. Hoffmann, The role of metal ion dopants in quantum-sized TiO_2: correlation between photoreactivity and charge carrier recombination dynamics, J. Phys. Chem. 98 (1994) 13669–13679.
[22] N. Serpone, D. Lawless, J. Disdier, J.-M. Herrmann, Spectroscopic, photoconductivity, and photocatalytic studies of TiO_2 colloids: naked and with the lattice doped with Cr^{3+}, Fe^{3+}, and V^{5+} cations, Langmuir 10 (1994) 643–652.
[23] M.I Litter, J.A. Navío, Photocatalytic properties of iron-doped titania semiconductors, J. Photochem. Photobiol. A 98 (1996) 171–181.
[24] J. Zhang, L. Xiao, Y. Cong, M. Anpo, Preparation and characterization of multifunctional titanium dioxide photocatalysts, Top. Catal. 47 (2008) 122–130.
[25] J. Rocha, A. Ferreira, Z. Lin, M.W. Anderson, Synthesis of microporous titanosilicate ETS-10 from $TiCl_3$ and TiO_2: a comprehensive study, Micropor. Mesopor. Mater. 23 (1998) 253–263.
[26] Z. Ji, J. Warzywoda, A. Sacco Jr., Competitive nucleation and growth in seeded batch crystallization of titanosilicate ETS-10 using $Ti(SO_4)_2$, Micropor. Mesopor. Mater. 81 (2005) 201–210.
[27] T. Zhang, T. Oyama, A. Aoshima, H. Hidaka, J. Zhao, N.J. Serpone, Photooxidative N-demethylation of methylene blue in aqueous TiO_2 dispersions under UV irradiation, J. Photochem. Photobiol. A 140 (2001) 163–172.
[28] A. Mills, J. Wang, Photobleaching of methylene blue sensitized by TiO_2: an ambiguous system? J. Photochem. Photobiol. A 127 (1999) 123–134.
[29] M. Winter, WebElements. Available from: http://www.webelements.com/, 1993.
[30] P.D. Southon, R.F. Howe, Spectroscopic studies of disorder in the microporous titanosilicate ETS-10, Chem. Mater. 14 (2002) 4209–4218.
[31] B. Yilmaz, J. Warzywoda, A. Sacco Jr., Spectroscopic characterization of the quantum wires in titanosilicates ETS-4 and ETS-10, Nanotechnology 17 (2006) 4092–4099.
[32] S. Velu, N. Shah, T.M. Jyothi, S. Sivasanker, Effect of manganese substitution on the physicochemical properties and catalytic toluene oxidation activities of Mg–Al layered double hydroxides, Micropor. Mesopor. Mater. 33 (1999) 61–75.
[33] W.S. Kijlstra, E.K. Poels, A. Bliek, B.M. Weckhuysen, R.A. Schoonheydt, Characterization of Al_2O_3-supported manganese oxides by electron spin resonance and diffuse reflectance spectroscopy, J. Phys. Chem. B 101 (1997) 309–316.
[34] Z. Ji, M.N. Ismail, D.M. Callahan Jr., E. Pandowo, Z. Cai, T.L. Goodrich, K.S. Ziemer, J. Warzywoda, A. Sacco Jr., The role of silver nanoparticles on silver modified titanosilicate ETS-10 in visible light photocatalysis, Appl. Catal. B 102 (2011) 323–333.

[35] S. Matsuo, N. Sakaguchi, K. Yamada, T. Matsuo, H. Wakita, Role in photocatalysis and coordination structure of metal ions adsorbed on titanium dioxide particles: a comparison between lanthanide and iron ions, Appl. Surf. Sci. 228 (2004) 233–244.
[36] X. Yan, T. Ohno, K. Nishijima, R. Abe, B. Ohtani, Is methylene blue an appropriate substrate for a photocatalytic activity test? A study with visible-light responsive titania, Chem. Phys. Lett. 429 (2006) 606–610.
[37] A.L. Linsebigler, G. Lu, J.T. Yates Jr., Photocatalysis on TiO_2 surfaces: principles, mechanisms, and selected results, Chem. Rev. 95 (1995) 735–758.
[38] A.M. Shough, D.J. Doren, B. Ogunnaike, Transition metal substitution in ETS-10: DFT calculations and a simple model for electronic structure prediction, Chem. Mater. 21 (2009) 1232–1241.